ADVANCED MATERIALS TECHNOLOGIES
www.advmattechnol.de

High-Resolution Lithography for High-Frequency Organic Thin-Film Transistors

Ute Zschieschang, Hagen Klauk, and James W. Borchert*

Organic thin-film transistors are field-effect transistors comprising a semiconductor in the form of a thin, typically polycrystalline layer of conjugated organic molecules. Since organic transistors can often be fabricated at temperatures no higher than about 100 °C, they are potentially useful for flexible, large-area electronics applications. An important performance parameter of organic transistors is the transit frequency, which is the highest frequency at which the transistors can be operated. The transit frequency of organic transistors is determined in large part by the channel length and the parasitic gate-to-source and gate-to-drain overlap lengths. How small these dimensions can be made depends (at least in the case of transistors fabricated in the lateral device architecture) greatly on the resolution of the lithography method that is utilized for the patterning of the gate electrodes and the source and drain contacts. Patterning methods that have yielded organic transistors with lateral dimensions sufficiently small to provide transit frequencies above 10 MHz include photolithography, laser lithography, stencil lithography, and electron-beam lithography. In this review, these four lithography methods and their roles in the fabrication of high-frequency organic transistors, as well as their prospects for future improvements in the dynamic performance of organic transistors, will be illuminated.

1. Introduction

Field-effect transistors (FETs) are three-terminal microelectronic devices in which the density of mobile electronic charges in a semiconductor and thus the electric current flowing through the transistor can be modulated by a transverse electric field applied by means of a metallic gate electrode across a thin insulating layer (the gate dielectric). FETs are used to implement a variety of electronic functions, such as switching (digital circuits), amplification (analog circuits), transduction (sensors) and data storage (memory). The semiconductor most commonly employed in FETs is single-crystalline silicon, based on which approximately 10^{22} FETs are manufactured annually for microprocessors, graphics processors, memory, wireless communication and many other types of integrated circuits. The maximum process temperature during the fabrication of silicon FETs is close to 1000 °C, required for the post-implantation anneal. Since the gate dielectric of silicon FETs is an oxide (traditionally silicon dioxide produced by the thermal oxidation of silicon; more recently also atomic-layer-deposited hafnium oxide), these FETs are called metal-oxide-semiconductor FETs, or MOSFETs. The most advanced silicon MOSFETs have a physical gate length (not to be confused with the numerical "node" identifier) of about 10 nm and a physical gate-dielectric thickness of about 2 nm (or slightly below that).

To enable the fabrication of FETs on substrates other than silicon, a wide range of alternative semiconductors that can be deposited in the form of thin solid films onto arbitrary substrates by chemical vapor deposition (CVD), physical vapor deposition (PVD) or atomic layer deposition (ALD) have been developed.[1] These semiconductors include hydrogenated amorphous silicon (a-Si:H),[2] polycrystalline silicon[3] and amorphous or polycrystalline metal oxides, most notably zinc oxide and indium gallium zinc oxide (IGZO).[4] Such FETs are called thin-film transistors (TFTs). The main application of TFTs is in electronic systems that require transistors to be fabricated on mechanically flexible or optically transparent substrates and/or to be distributed over large areas (e.g., larger than a silicon wafer). Examples for TFT applications are active-matrix displays[5] and active-matrix sensor or detector arrays.[6] These are usually fabricated on glass or polyimide substrates by the sequential deposition and patterning of all the functional materials. The maximum process temperature for the fabrication of high-performance TFTs based on inorganic semiconductors ranges from about 150 °C for metal-oxide TFTs[7] to about 250 °C for amorphous-silicon TFTs[8] to about 425 °C for low-temperature polycrystalline-silicon (LTPS) TFTs.[9]

U. Zschieschang, H. Klauk
Max Planck Institute for Solid State Research
Heisenbergstr. 1, 70569 Stuttgart, Germany
E-mail: h.klauk@fkf.mpg.de

J. W. Borchert
1st Institute of Physics
Georg August University of Göttingen
Friedrich-Hund-Platz 1, 37077 Göttingen, Germany

The ORCID identification number(s) for the author(s) of this article can be found under https://doi.org/10.1002/admt.202201888

DOI: 10.1002/admt.202201888

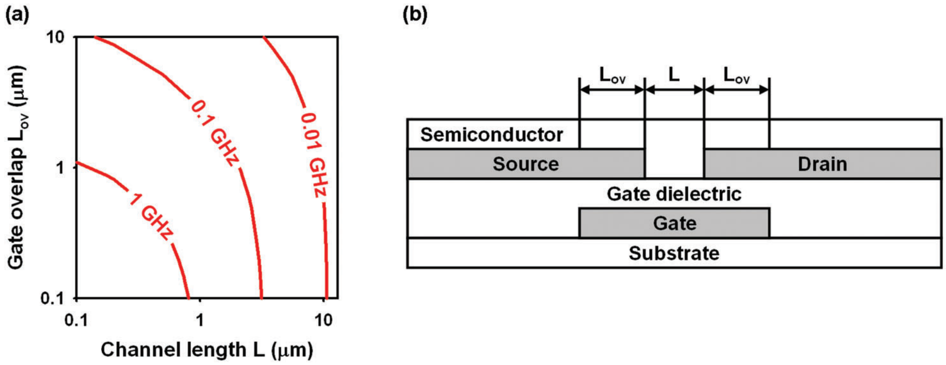

Figure 1. a) Contour plot showing the transit frequency (f_T) calculated using Equation (1) and plotted as a function of the channel length (L) and the gate-to-contact overlap (L_{ov}) for the following parameter values: $\mu_0 = 10$ cm^2 V^{-1}s^{-1}, $R_C W = 10$ Ωcm, $V_{GS} - V_{th} = 5$ V, $C_{diel} = 0.1$ µF cm^{-2}. As can be seen, the transit frequency has a strong dependence on the channel length (L) and the gate-to-contact overlaps (L_{ov}). b) Schematic cross-section of an organic transistor in the lateral, inverted coplanar (bottom-gate, bottom-contact) device architecture.

TFTs can also be fabricated using organic semiconductors. These are conjugated, van-der-Waals-bound hydrocarbons that can be broadly categorized into polymers and small-molecule semiconductors and which are typically produced by synthetic protocols.[10] The fabrication of organic TFTs is often possible at process temperatures no higher than approximately 100 °C, which means they can be fabricated on a wide range of temperature-sensitive, inexpensive and/or biodegradable substrates, such as polyethylene naphthalate,[11] textiles[12] or paper.[13]

An important transistor-performance parameter is the transit frequency (f_T), which is the highest frequency at which the transistor can amplify electrical signals and which is given by the ratio between the transconductance and the overall gate capacitance. For example, the TFTs that are used to implement the pixel circuits in active-matrix displays need to have transit frequencies on the order of a few hundred kilohertz to a few tens of megahertz, depending on the display resolution and the frame rate. If the TFTs are also employed to implement the row and column drivers of the displays,[14] an even higher transit frequency is required.

The transit frequency of an FET operated in the saturation regime is given by the following equation, derived using the Meyer capacitance model:[15]

$$f_T = \frac{\mu_0 \left(\left|V_{GS} - V_{th}\right|\right)}{\left(1 + \frac{\mu_0 \left(\left|V_{GS} - V_{th}\right|\right) C_{diel} R_C W}{2L}\right) 2\pi L \left(\frac{2}{3} L + 2 L_{ov}\right)} \tag{1}$$

where μ_0 is the intrinsic channel mobility, V_{GS} is the gate-source voltage, V_{th} is the threshold voltage, C_{diel} is the unit-area gate-dielectric capacitance, R_C is the contact resistance, W is the channel width, L is the channel length, and L_{ov} is the gate-to-contact overlap (assuming equal gate-to-source and gate-to-drain overlap lengths).

Figure 1a illustrates the dependence of the transit frequency on the critical TFT dimensions (L and L_{ov}) calculated using Equation (1). For these calculations, the other TFT parameters were set to the following values: $\mu_0 = 10$ cm^2 V^{-1}s^{-1}; $R_C W = 10$ Ωcm; $V_{GS} - V_{th} = 5$ V; $C_{diel} = 0.1$ µF cm^{-2}. These values either represent approximately the state-of-the-art for organic TFTs in terms of charge-carrier mobility[16] and contact resistance,[17] or they reflect approximately the requirements in terms of the maximum supply voltage available in mobile electronics applications (powered by small batteries or energy-harvesting devices). Figure 1a illustrates the enormous incentive of decreasing the channel length (L) and the gate-to-contact overlaps (L_{ov}) for improving the dynamic performance of organic TFTs. For channel lengths and gate-to-contact overlaps below about 0.5 µm, the transit frequency of organic TFTs approaches and may possibly exceed 1 GHz.

How small the channel length and the gate-to-contact overlaps can be made depends critically on the device architecture and the patterning method. Regarding the device architecture, organic TFTs can be categorized into vertical transistors and lateral transistors. In vertical transistors, the channel length is determined by the thickness of a deposited layer (typically either the thickness of the semiconductor or the thickness of an insulating spacer or mesa structure separating the source and drain contacts). The technology and the properties of vertical organic transistors have been expertly and comprehensively reviewed on several occasions[18–20] and will thus not be considered here.

In lateral transistors, the channel length and the gate-to-contact overlaps are defined by the lateral distance between the edges of the source and drain contacts (L) and by the lateral overlap of the gate electrode with respect to the source and drain contacts (L_{ov}; see Figure 1b). Therefore, both the channel length and the gate-to-contact overlaps of lateral transistors are defined by the lithographic patterning of the gate electrodes and the source and drain contacts. The lithographic techniques that have been employed in the fabrication of high-frequency lateral organic TFTs will be the focus of this review.

To date, lateral organic TFTs with operation frequencies above 10 MHz have been fabricated using four different lithography methods: photolithography, laser lithography, stencil lithography, and electron-beam lithography. In the following, these methods and their roles in the fabrication of high-frequency organic TFTs as well as their prospects for future improvements in the dynamic performance of organic TFTs will be discussed. For the purpose of this review, the term "lithography" will be defined as any method employed to pattern the various TFT components, in particular the gate electrodes and the source and drain contacts, regardless of whether this is accomplished with or without the help of masks or resists, and regardless of whether the pattern is produced in an additive or subtractive manner.

2. Photolithography

Photolithography was the first patterning method to yield organic TFTs with transit frequencies above 10 MHz. In photolithography, a layer of a photosensitive polymer (the photoresist) is uniformly deposited onto the substrate and then exposed to ultraviolet radiation through either a photomask containing the desired pattern (mask-based photolithography) or a digital light modulator (maskless photolithography). The resist pattern is then developed using an aqueous alkaline solution, which dissolves and removes the exposed regions of the resist. Alternatively, a negative-tone-resist process can be employed, in which case the unexposed resist regions are dissolved and removed. Pattern transfer from the photoresist to the functional material is then accomplished either by etching or by lift-off. For pattern transfer by etching, the functional material is deposited prior to the photoresist, which then serves as an etch mask during the subsequent dry or wet-chemical etching of the functional material, followed by removing (stripping) the photoresist using an organic solvent. For pattern transfer by lift-off, the functional material is deposited over the patterned photoresist, which is then lifted-off along with the excess material using an organic solvent.

Photolithography has been the key enabler for the efficient commercial manufacturing of microelectronic devices and integrated circuits since the 1960s and has seen unremitting improvements over the past six decades.[21] It is important to distinguish between contact lithography (where the photomask is in physical contact with the photoresist during exposure), proximity lithography (where the photomask is held in close proximity of the photoresist), projection lithography (where the photomask pattern is reduced in size and projected onto the resist using a system of lenses), and maskless lithography (where the pattern is generated digitally and then optically reduced and projected). Projection lithography with a radiation wavelength of 248 nm (KrF laser), 193 nm (ArF laser), or 13.5 nm (Sn plasma excited by a CO_2 laser) is routinely performed in the commercial manufacturing of silicon MOSFETs and provides a resolution as small as about 10 nm. However, the costs associated with advanced projection lithography are enormous, and there are no reports so far of organic TFTs fabricated using projection photolithography.

Contact, proximity, and maskless photolithography are usually performed with a radiation wavelength of 365 nm (Hg vapor lamp) or 375 nm (diode laser) and with the help of comparatively simple and affordable exposure systems. These methods are thus frequently utilized for the fabrication of organic TFTs. The lateral resolution that can be obtained with these approaches is on the order of 1 µm.

High-frequency organic TFTs have been fabricated by photolithography primarily in the inverted coplanar (bottom-gate, bottom-contact) and in the inverted staggered (bottom-gate, top-contact) device architectures. The inverted coplanar architecture has the advantage that the gate electrodes and the source and drain contacts are deposited and patterned prior to the deposition of the semiconductor, thus avoiding any exposure of the organic semiconductor to potentially harmful solvents, developers or etchants during the patterning of the gate electrodes and the source and drain contacts.[22] In 2009 and 2011, Masatoshi Kitamura and Yasuhiko Arakawa (University of Tokyo) reported n-channel and p-channel organic TFTs fabricated in the inverted coplanar device architecture with gate electrodes and source and drain contacts patterned using a combination of photolithography and lift-off, and using the vacuum-deposited small-molecule organic semiconductors C_{60} (for the n-channel TFTs) and pentacene (for the p-channel TFTs).[23,24] These TFTs had a channel length of 2 µm, gate-to-contact overlaps as small as 1 µm, and a channel-width-normalized contact resistance as small as 940 Ωcm, ultimately enabling transit frequencies up to 27.7 MHz. This was by far the best dynamic performance reported for organic TFTs at the time and remained the result to beat for nearly a decade.

The use of photolithography in combination with the inverted coplanar device architecture has also led to the demonstration of organic-TFT-based integrated circuits and active-matrix organic light-emitting diode (AMOLED) displays with impressive characteristics. For example, Kris Myny et al. (imec, Leuven) reported on the fabrication of ring oscillators with a signal propagation delay of 400 ns per stage,[25] a 64-bit radio-frequency identification transponder with a data rate of 4.3 kbit s^{-1},[26] and an 8-bit microprocessor consisting of 3381 organic TFTs with an integration density of 1000 TFTs/cm^2.[27] Daniele Raiteri et al. (Technical University Eindhoven) designed, fabricated and characterized a 240-stage shift register consisting of 13 440 organic TFTs with an integration density of 2000 TFTs/cm^2.[28] Makoto Noda et al. (Sony Corp., Atsugi) demonstrated a rollable, full-color AMOLED display composed of 311 040 pixels (432 rows, 240 columns, RGB) with a display resolution of 121 ppi (pixels per inch), 622 080 organic TFTs (two TFTs per pixel) and an integration density of 13 600 TFTs/cm^2.[29] All these circuits and displays were based on organic TFTs with channel lengths between 2 and 5 µm and were fabricated on flexible polymeric substrates using photolithography. **Figure 2** illustrates some of the results of this work.

One drawback of the inverted coplanar device architecture is that it presents an uneven surface for the deposition of the organic semiconductor, since the presence of the source and drain contacts on the gate dielectric can create a topography as well as a contrast in surface energy. Both of these aspects may create challenges for the deposition of the organic-semiconductor layer, especially if it is deposited using a surface-sensitive technique, such as solution-shearing or edge-casting.[30] These challenges can be avoided by fabricating the TFTs in the inverted staggered (bottom-gate, top-contact) device architecture, where the organic-semiconductor layer is deposited onto the smooth and uniform gate-dielectric surface, followed by the deposition of the source and drain contacts. The damage potentially imposed on the organic semiconductor by the photolithographic patterning of the source and drain contacts on its surface can be minimized by employing orthogonal photolithography, which was proposed by George Malliaras and Christopher Ober in 2009 and is based on fluorinated photoresists and fluorous solvents.[31]

The use of orthogonal photolithography for the fabrication of high-frequency organic TFTs in the inverted staggered device architecture was perfected by the group of Jun Takeya (University of Tokyo). They successfully employed orthogonal photolithography in combination with either wet-chemical etching[32–34] or

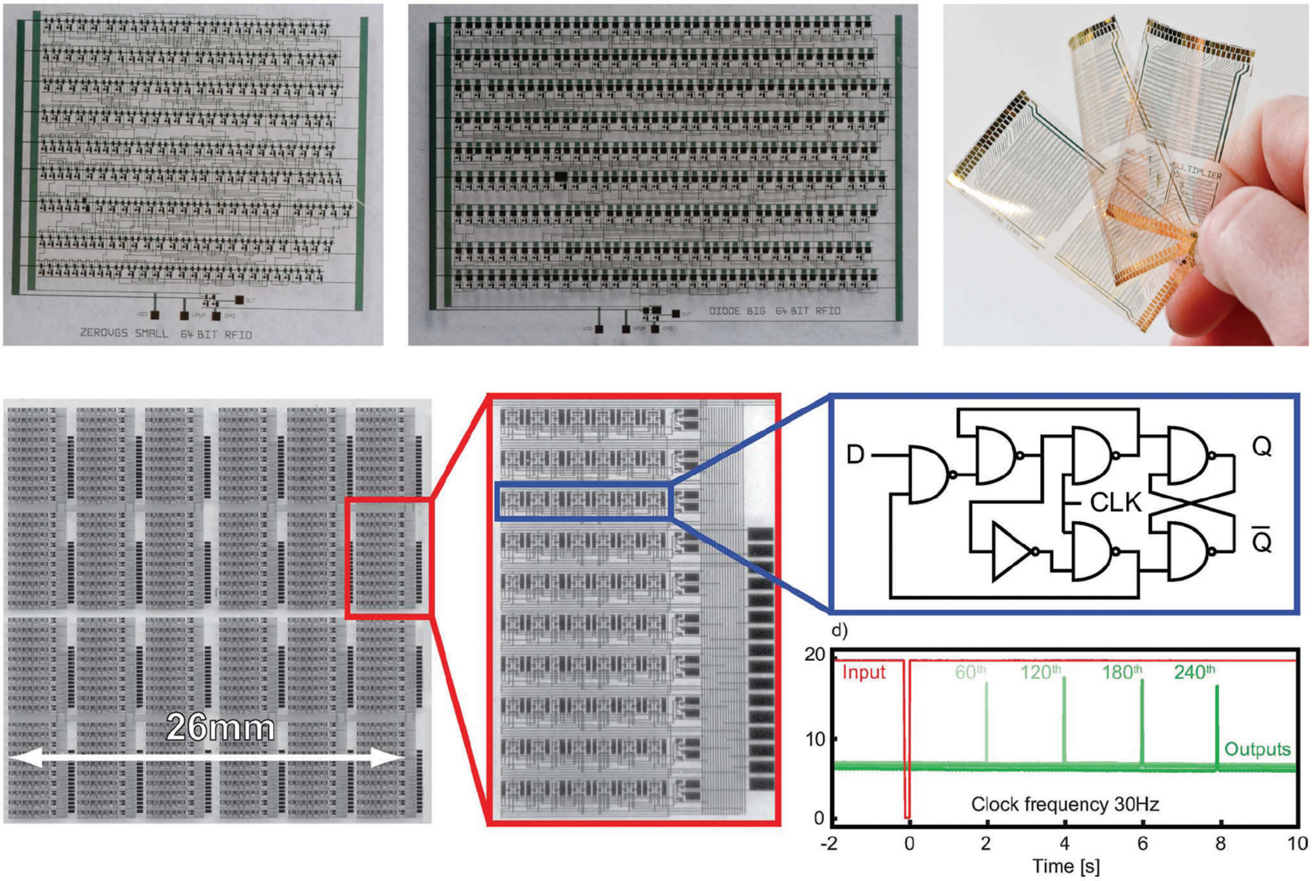

Figure 2. Photolithography for flexible circuits and rollable displays based on organic TFTs. Top: 64-bit transponders and 8-bit microprocessor by Kris Myny et al. Adapted with permission.[26,27] Copyright 2011, IEEE; 2012, IEEE. Bottom: 240-stage shift register by Daniele Raiteri et al.). Adapted with permission.[28] Copyright 2014, IEEE.

Table 1. Literature summary of organic TFTs fabricated using photolithography for which operation at frequencies above 10 MHz has been reported.

Author	Ref.	Substrate	Semiconductor	f_T or f_{eq} [MHz]	L [µm]	L_{ov} [µm]	μ_0 [cm^2 V^{-1}s^{-1}]	$R_C W$ [Ωcm]	V_{GS} [V]	V_{th} [V]	C_{diel} [nF cm^{-2}]
Kitamura	[23]	Glass	C_{60}	20	2	1	n/a	n/a	20	8.6	20
Kitamura	[24]	Glass	C_{60}	27.7	2	2.5	n/a	940	20	9	20
Kitamura	[24]	Glass	Pentacene	11.4	2	2.5	n/a	3000	−20	−4	20
Nakayama	[32]	Glass	C_{10}-DNTT	19	2	2	5	200	−10	0	77
Yamamura	[33]	Glass	C_8-DNBDT-NW	20	3	2.25	3.3	47	−10	−5	80
Sawada	[34]	Glass	C_9-DNBDT-NW	45	1.5	1	10.7	60	−7	1	130
Yamamura	[35]	Glass	C_9-DNBDT-NW	38	1.5	2	11	47	−15	−3	36

lift-off of the gold source and drain contacts.[35] In most cases, the organic semiconductors were deposited by edge-casting, with a thickness precisely controlled to one, two or three molecular monolayers.[33] The small thickness of the semiconductor layer is helpful in minimizing the TFTs' contact resistance, and its vanishingly small surface roughness is beneficial in facilitating the high-resolution patterning of the source and drain contacts on the semiconductor surface. Organic dopants, such as F_4-TCNQ and F_6-TNAP, were employed to alleviate the detrimental influence of resist residue at the interface between the organic-semiconductor layer and the source/drain contacts on the contact resistance.[33–35] These TFTs had channel lengths as small as 1.5 µm, gate-to-contact overlaps as small as 1 µm, a contact resistance as small as 47 Ωcm, and transit frequencies up to 45 MHz. The latter is the highest transit frequency reported to date for lateral organic TFTs at supply voltages below 10 V. **Table 1** provides a summary of the key parameters of high-frequency organic TFTs fabricated using photolithography, and **Figure 3** illustrates some of the reported results.

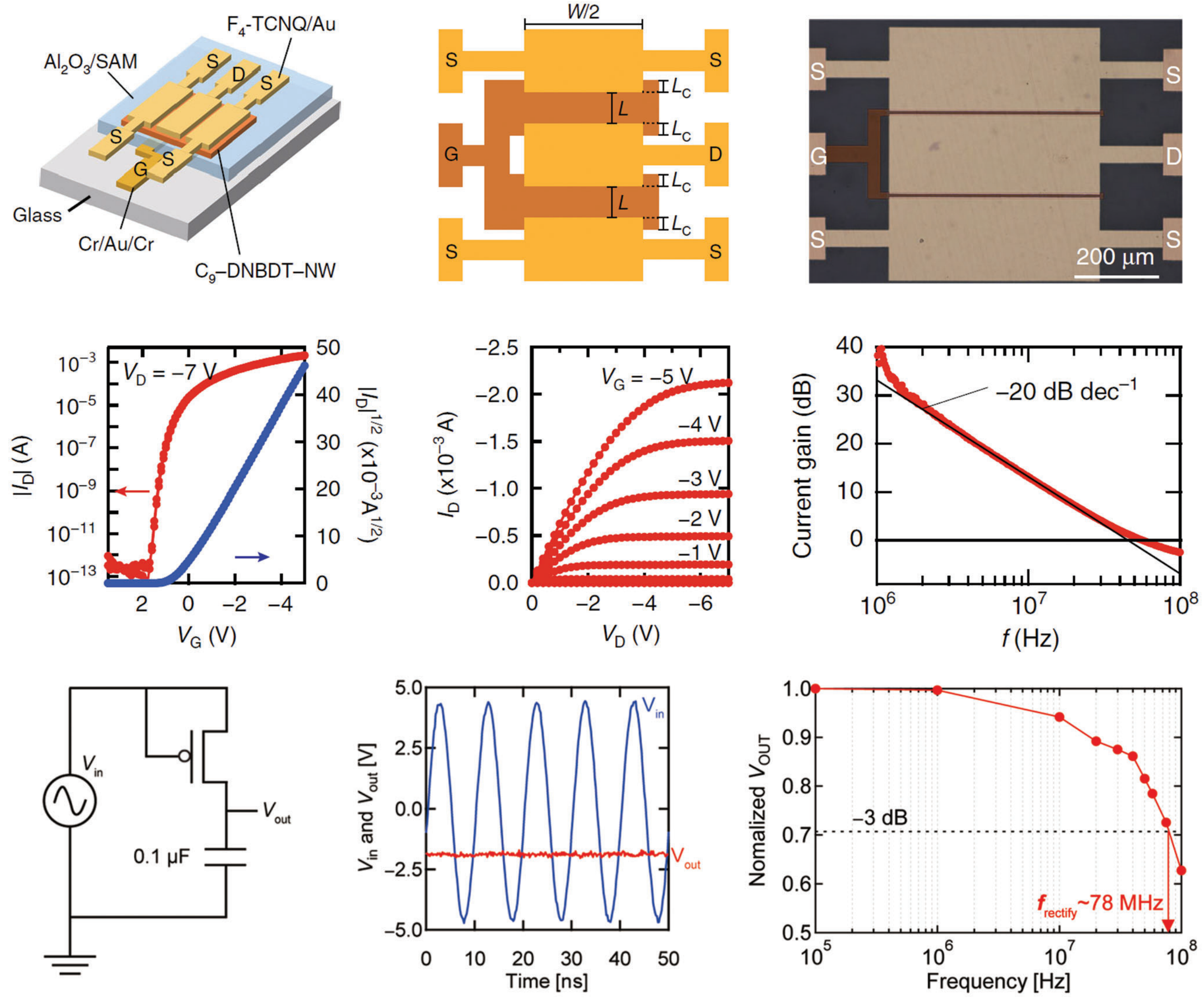

Figure 3. Photolithography for high-frequency organic TFTs, fabricated in the inverted staggered (bottom-gate, top-contact) device architecture with channel lengths as small as 1.5 µm, gate-to-contact overlaps as small as 1 µm, transit frequencies up to 45 MHz, and rectification frequencies up to 78 MHz (Taiki Sawada et al.; Akifumi Yamamura et al.). Top and center: Adapted under the terms of the CC BY license.[34] Copyright 2020, American Association for the Advancement of Science. Bottom: Adapted with permission.[35] Copyright 2020, Wiley-VCH.

One of the key advantages and the main reason for the unparalleled success of photolithography in global semiconductor manufacturing is its potentially very high throughput, which is owed to the fact that the entire substrate (or at least an entire chip, as in the case of projection lithography) is exposed at once and within a very short amount of time, usually no more than a few seconds. Photolithography can provide high throughput regardless of whether it is performed with or without masks. Maskless photolithography avoids the often substantial costs for the fabrication of photomasks and is thus useful for rapid prototyping (and for mask fabrication), while mask-based photolithography is often the preferred choice for high-volume manufacturing.

Another useful feature of photolithography is that it lends itself naturally to the self-alignment of the source and drain contacts with respect to the gate electrode by means of a backside exposure during which the gate electrode serves as a photomask for the patterning of the source and drain contacts.[36] Provided the substrate is sufficiently transparent and the gate material is sufficiently opaque for radiation at the exposure wavelength, this method provides a cost-effective and high-throughput approach to the quasi-elimination of the gate-to-source and gate-to-drain overlaps. Organic TFTs with gate-to-source and gate-to-drain overlaps as small as 25 nm and transit frequencies as high as 3.3 MHz have been reported by the groups of Barbara Stadlober (Joanneum Research)[37] and Alasdair Campbell (Imperial College London).[38] **Figure 4** illustrates some of the results of the fabrication of organic TFTs with vanishingly small gate-to-contact overlaps achieved with the help of self-aligned photolithography.

The main drawback of photolithography is that it necessitates the use of resists, organic solvents, and possibly etchants. Aside from the environmental and health aspects associated with the production and disposal of large amounts of these substances,

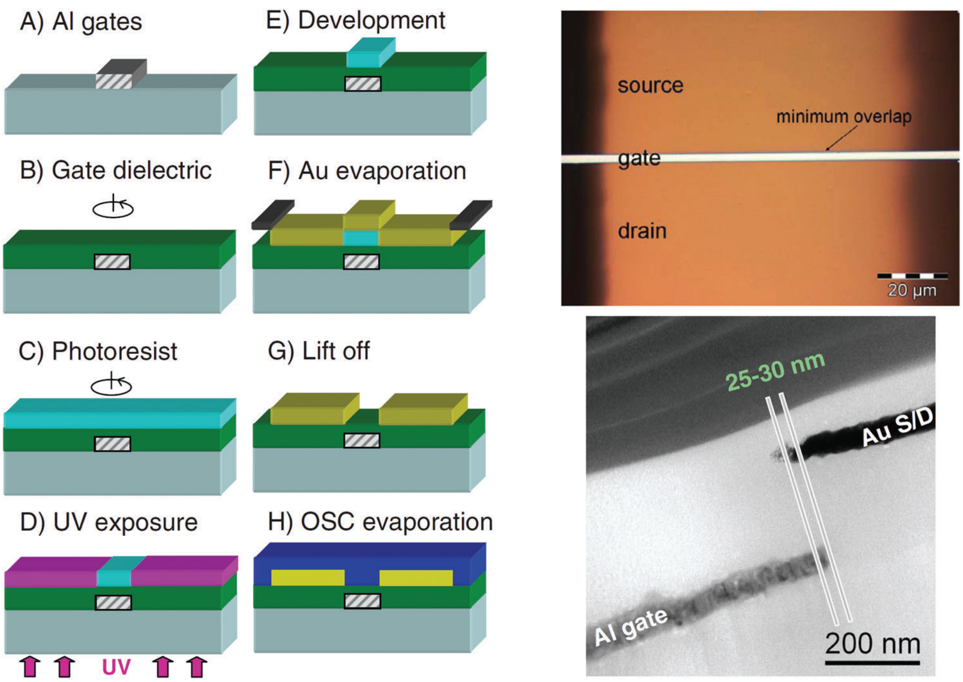

Figure 4. Self-aligned photolithography for organic TFTs with extremely small gate-to-contacts overlaps, accomplished using a backside exposure during which the gate electrode serves as a photomask for the patterning of the source and drain contacts (Ursula Palfinger et al.). Adapted with permission.[37] Copyright 2010, Wiley-VCH.

problems may arise when these materials come into contact with the organic-semiconductor layer during the device fabrication (although the latter issue can be alleviated through the use of orthogonal photolithography, as mentioned above, or dry-film photoresists).

The minimum resolution achievable using photolithography depends on the details of the method. Generally speaking, contact and maskless photolithography provide a resolution on the order of 1 µm in the photoresist. Note that this is not necessarily the minimum achievable channel length. For example, if the source/drain metal is patterned by isotropic etching, the resulting physical channel length will be somewhat larger than the feature size in the resist, due to the unavoidable underetching. The wet-chemical etching of metals is typically isotropic. Anisotropic metal etching is in principle possible with dry (plasma) etching, although this has never been reported for organic TFTs.

For a channel length of 1 µm and gate-to-contact overlaps of either 1 µm (i.e., without self-alignment) or zero (perfect self-alignment), Equation (1) predicts transit frequencies on the order of 200 MHz or 1 GHz, respectively (assuming $\mu_0 = 10$ cm^2 V^{-1}s^{-1}; $R_C W = 10$ Ωcm; $V_{GS} - V_{th} = 5$ V; $C_{diel} = 0.1$ µF cm^{-2}).

3. Laser Lithography

The use of high-resolution laser lithography for the fabrication of high-frequency organic TFTs was developed by the group of Mario Caironi (IIT Milano) and was first reported in 2016.[39] In this process, a femtosecond laser is utilized for the precise area-selective sintering of a thin layer of metal nanoparticles to define the source and drain contacts of the TFTs (in some cases also the gate electrodes). In the first step of this process, the substrate is uniformly coated with a layer of metal (usually silver) nanoparticles. The nanoparticles have an average diameter of about 20 nm, the film is typically deposited by spin-coating, and the resulting film thickness is about 70 nm. The focused beam of a femtosecond laser (gain medium: Yb:KGd$(WO_4)_2$; emission wavelength: 1030 nm; repetition rate: 67 MHz; pulse duration: 80 fs; beam power density: 1.9 mW cm^{-2}) is then scanned with a rate of about 50 to 100 µm s^{-1} across those regions of the substrate in which the source and drain contacts need to be defined. The absorbed laser radiation locally heats and sinters the nanoparticles, thereby rendering the nanoparticle film electrically conducting in the exposed regions. The substrate is then rinsed with water or a mild solvent to remove the nanoparticles outside of the laser-exposed regions, leaving behind the patterned metal source and drain contacts on the substrate surface.

The resolution achievable with this method is likely limited by the radiation wavelength, the laser-beam diameter, and/or the thermal and mechanical properties of the metal-nanoparticle film. Organic TFTs with a channel length as small as 1 µm have been reported.[40] The TFTs have so far all been fabricated in the top-gate staggered device architecture, that is, the source and drain contacts were patterned by laser lithography on the substrate surface, followed by the deposition of the organic semiconductor, the gate dielectric and the gate electrodes. In early reports,[39–42] the gate electrodes were patterned by inkjet-printing, resulting in gate-to-contact overlaps of about 2 to 3 µm and transit frequencies up to 24 MHz.[42] More recently, the gate electrodes were fabricated by laser lithography as well, resulting in gate-to-contact overlaps as small as 130 nm and a record-high transit frequency of 160 MHz.[43] These transistors had a channel-width-normalized contact resistance of 300 Ωcm

Table 2. Literature summary of organic TFTs fabricated using laser lithography for which operation at frequencies above 10 MHz has been reported.

Author	Ref.	Substrate	Semiconductor	f_T or f_{eq} [MHz]	L [µm]	L_{ov} [µm]	μ_0 [cm^2 V^{-1}s^{-1}]	$R_C W$ [Ωcm]	V_{GS} [V]	V_{th} [V]	C_{diel} [nF cm^{-2}]
Perinot	[39]	Glass	P(NDI2OD-T2)	20	1.75	3	n/a	7300	30	0	6
Perinot	[40]	Flexible PEN	P(NDI2OD-T2)	14.4	1	1.7	0.3	1015	7	0.5	39
Giorgio	[41]	Glass	P(NDI2OD-T2)	19	1.2	2.3	1	1000	12	1	27
Passarella	[42]	Glass	DPPT-TT	24	1.4	2.7	n/a	n/a	−15	0	8
Passarella	[42]	Flexible PEN	DPPT-TT	22	1.2	2.3	n/a	n/a	−12	0	8
Perinot	[43]	AlN	P(NDI2OD-T2)	160	1.2	0.17	1	300	40	0	8.54

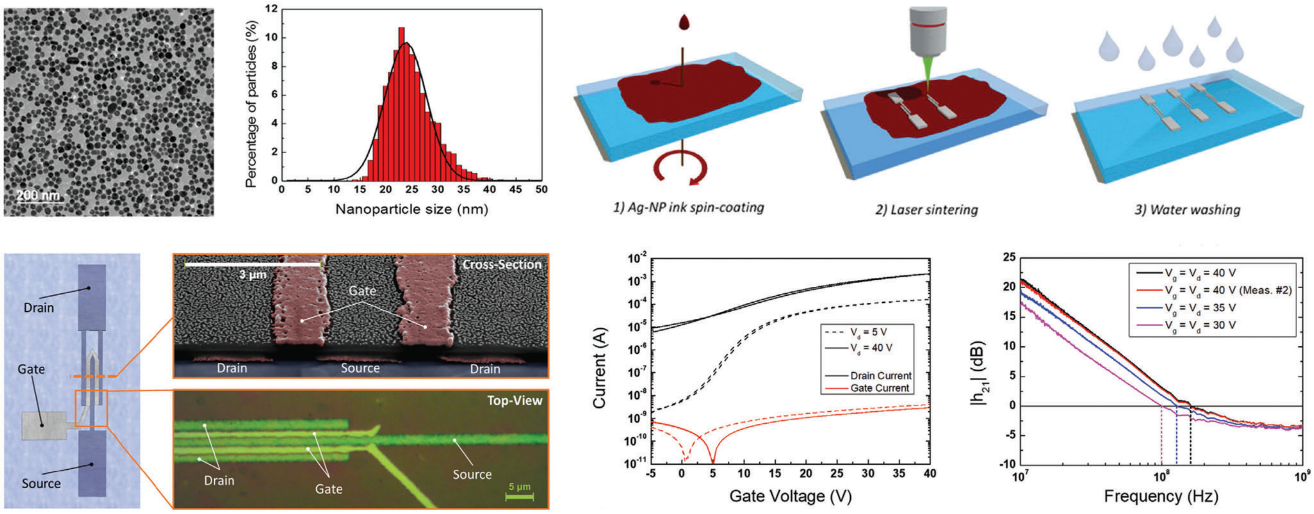

Figure 5. Laser lithography for high-frequency organic TFTs, fabricated in the top-gate staggered device architecture with channel lengths as small as 1 µm, gate-to-contact overlaps as small as 0.17 µm, and transit frequencies up to 160 MHz (Andrea Perinot et al.). Adapted under the terms of the CC-BY license.[39,43] Copyright 2016, Springer Nature; 2021, Wiley-VCH.

(which is likely the parameter limiting the transit frequency in this case). **Table 2** provides a summary of the key parameters of high-frequency organic TFTs fabricated using laser lithography, and **Figure 5** illustrates some of the reported results.

The laser-lithography method developed by the group of Mario Caironi is strictly a direct-write, maskless patterning technique. Its main advantages are the high resolution and the fact that it does not require masks, resists, etchants or solvents, aside from the liquids to disperse and remove the nanoparticles. Drawbacks include the high costs associated with the femtosecond laser system and the low throughput of single-beam laser systems. For a channel length of 1 µm and gate-to-contact overlaps of 100 nm, Equation (1) predicts a transit frequency of 700 MHz (assuming $\mu_0 = 10$ cm^2 V^{-1}s^{-1}; $R_C W = 10$ Ωcm; $V_{GS} - V_{th} = 5$ V; $C_{diel} = 0.1$ µF cm^{-2}).

4. Stencil Lithography

Stencil lithography is an additive, all-dry patterning technique whereby the functional materials are deposited by vacuum evaporation or sublimation through openings in a membrane (the stencil mask) positioned in close proximity of (or in direct contact with) the substrate.[44] In stencil lithography, the functional materials are deposited onto the substrate only where needed for the devices and circuits, which eliminates the requirement for subtractive patterning and avoids the exposure of any materials already present on the substrate to potentially harmful resists, solvents, etchants, radiation or heat. For this reason, stencil lithography is currently the only viable method for the fabrication of organic light-emitting diodes in commercially manufactured AMOLED displays,[45] used primarily in about 600 million mobile phones currently produced annually. The stencil masks employed in commercial AMOLED manufacturing are made of a metal (usually Invar, which has a thermal expansion coefficient of zero) and are thus referred to as "fine metal masks." The openings in fine metal masks are typically created by water-jet-guided laser cutting[46] and provide a minimum feature size on the order of 10 µm, which is sufficient for a maximum display resolution of about 600 ppi (pixels per inch).

Alternatives to metal masks are silicon or silicon-nitride membranes manufactured on the surface of a silicon wafer either by photolithography, by focused ion beam milling[47] or by a combination of electron-beam lithography and deep reactive-ion etching.[48] Silicon stencil masks were originally developed in the 1990s for ion-projection lithography,[49] which was under consideration as one of the next-generation lithography techniques

Table 3. Literature summary of organic TFTs fabricated using stencil lithography for which operation at frequencies above 10 MHz has been reported.

Author	Ref.	Substrate	Semiconductor	f_T or f_{eq} [MHz]	L [µm]	L_{ov} [µm]	μ_0 [cm^2 V^{-1}s^{-1}]	$R_C W$ [Ωcm]	V_{GS} [V]	V_{th} [V]	C_{diel} [nF cm^{-2}]
Borchert	[52]	Flexible PEN	DPh-DNTT	21	0.6	5	6	10	−3	−1	700
Zschieschang	[53]	Flexible PEN	DPh-DNTT	10.4	0.85	5	5	30	−3	−0.7	700

intended to eventually replace photolithography in silicon-MOSFET manufacturing (a race ultimately won by extreme-ultraviolet lithography). Silicon stencil masks can provide sub-micrometer resolution and were first utilized for the fabrication of organic TFTs in 2010 in the group of Jürgen Brugger (EPFL).[50]

In 2012, Tarek Zaki et al. (IMS CHIPS, Stuttgart) reported on the design and fabrication of a 6-bit digital-to-analog converter based on organic TFTs. The circuit was fabricated on a glass substrate using a set of four silicon stencil masks (one each for the interconnects, the gate electrodes, the organic semiconductor, and the source/drain contacts). The organic TFTs had a channel length of 4 µm and gate-to-contact overlaps of 20 µm. The converter was designed in a current-steering circuit architecture and operated with a data conversion rate of up to 100 kS s^{-1}.[51] This data rate was achieved with a supply voltage of 3.3 V and is still the highest data rate reported for an organic-TFT-based data converter. The TFTs were fabricated in the inverted staggered (bottom-gate, top-contact) device architecture and had a channel-width-normalized contact resistance of about 100 Ωcm.[15]

In 2020, James W. Borchert et al. reported on the fabrication of organic TFTs in the inverted coplanar (bottom-gate, bottom-contact) device architecture with channel lengths as small as 0.6 µm and gate-to-contact overlaps as small as 2 µm on flexible polyethylene naphthalate (PEN) substrates using silicon stencil masks. These TFTs exhibited a channel-width-normalized contact resistance of 10 Ωcm, a channel-width-normalized transconductance up to 6.4 S m^{-1}, transit frequencies up to 21 MHz, and a signal propagation delay of 79 ns per stage measured on an 11-stage ring oscillator operated with a supply voltage of 4.4 V.[52,53] Long-channel TFTs ($L = 8$ µm) showed an on/off current ratio of 10^{10} and a subthreshold swing of 59 mV/decade (measured at a temperature of 292 K). At the time of publication, most of these parameters represented records for flexible organic TFTs. The results of this work are summarized and illustrated in **Table 3** and **Figures 6** (individual TFTs) and **7** (integrated circuits). A comprehensive analysis of the dynamic characteristics of these TFTs was provided by Jakob Leise et al., using a compact model based on a closed-form description of the frequency-dependent small-signal gain accurately accounting for all relevant secondary effects, such as contact resistance, charge traps, fringe capacitances, subthreshold regime and non-quasistatic effects.[54]

According to a detailed analysis by Oscar Vazquez-Mena et al. of the blurring that occurs when a material is deposited onto a surface through openings in a stencil mask, the resolution limit of stencil lithography is about 0.2 µm.[55] This value therefore represents approximately the smallest channel length that can realistically be expected when using stencil lithography. The smallest channel length that has been reported for organic TFTs fabricated using stencil lithography is 0.3 µm.[56] The smallest total gate-to-contact overlap (sum of gate-to-source and gate-to-drain overlaps) reported for organic TFTs fabricated using stencil lithography is 4 µm.[52,57]

In the previous sections of this review, whenever Equation (1) was used to predict the transit frequency, the gate-overdrive voltage ($V_{GS} - V_{th}$) and the unit-area gate-dielectric capacitance (C_{diel}) were always set to values of 5 V and 0.1 µF cm^{-2}, respectively. Using these values (and again assuming $\mu_0 = 10$ cm^2 V^{-1}s^{-1} and $R_C W = 10$ Ωcm), Equation (1) predicts a transit frequency of 300 MHz for a channel length of 0.3 µm and gate-to-contact overlaps of 2 µm. However, the TFTs fabricated using stencil lithography mentioned above[52,53,56,57] had a unit-area gate-dielectric capacitance of 0.7 µF cm^{-2} and were operated with a gate-overdrive voltage of about 2 V. For these values ($L = 0.3$ µm, $L_{ov} = 2$ µm; $\mu_0 = 10$ cm^2 V^{-1}s^{-1}; $R_C W = 10$ Ωcm; $V_{GS} - V_{th} = 2$ V; $C_{diel} = 0.7$ µF cm^{-2}), Equation (1) predicts a transit frequency of 70 MHz.

In addition to its advantage of being an all-dry patterning technique, stencil lithography also eliminates the need for radiation sources and complex optical systems, aside from a vision system to enable mask alignment. One of the drawbacks of stencil lithography is the high cost of the masks, which are typically more difficult to manufacture than the photomasks employed for contact and proximity photolithography. Another drawback of stencil lithography is the limitation in terms of the mask size, which is dictated by the limited mechanical stability of the membranes; the stability and thus the maximum size of the membranes can be increased by increasing the membrane thickness, but this would compromise the achievable resolution.

5. Electron-Beam Lithography

The most recent addition to the family of high-resolution lithography techniques to have found use in the fabrication of organic TFTs with transit frequencies above 10 MHz is electron-beam lithography. In electron-beam lithography, the desired pattern is written into a layer of poly(methyl methacrylate) (PMMA) using a focused electron beam and developed by dissolving the exposed PMMA using a weak organic solvent. Unlike photoresists, whose photosensitivity is the result of blending the polymer with a photosensitizer, the sensitivity of PMMA to electron-beam exposure is intrinsic and due to radiation-induced polymer-chain scission. Depending on the characteristics of the electron beam and the PMMA properties, this potentially allows for a lateral resolution of better than 5 nm.[58] Pattern transfer from the PMMA resist to the functional material is usually accomplished by lift-off.

The use of electron-beam lithography for the fabrication of organic TFTs was pioneered by the groups of Dan Frisbie (University of Minnesota), Dominique Vuillaume (CNRS), George Malliaras (Cornell University), Ananth Dodabalapur (University of Texas), and Vivek Subramanian (UC Berkeley).[59–64] These

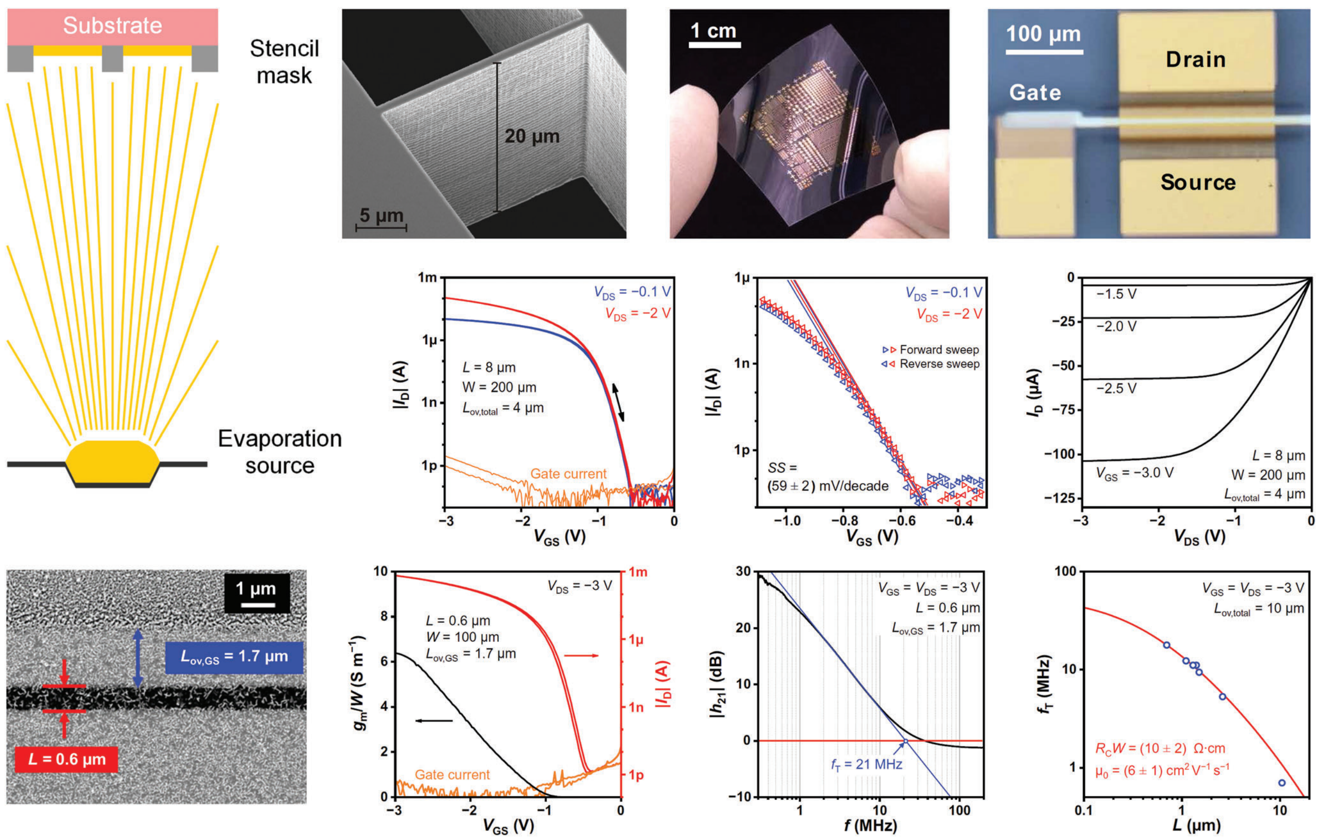

Figure 6. Stencil lithography for high-frequency organic TFTs, fabricated on flexible polymeric substrates in the inverted coplanar (bottom-gate, bottom-contact) device architecture with channel lengths as small as 0.6 µm and transit frequencies up to 21 MHz (Tarek Zaki et al.; James Borchert et al.). Stencil-mask photograph: Adapted with permission.[51] Copyright 2012, IEEE. All other images: Adapted under the terms of the CC BY-NC license.[52] Copyright 2020, American Association for the Advancement of Science.

early contributions already produced functional organic TFTs with channel lengths as small as about 10 nm.[62,63] For simplicity, these TFTs were fabricated on silicon substrates, a configuration in which the doped silicon also serves as a global gate electrode for all transistors on the substrate, so that only the source and drain contacts need to be patterned. The drawback of this configuration is that it prevents the transistors from being integrated into circuits and that it limits the dynamic TFT response, due to the parasitic capacitances associated with the overlaps of the source and drain contacts with the conducting substrate. A transit frequency of 2 MHz was reported in 2006 for organic TFTs with a channel length of 480 nm fabricated on silicon substrates using electron-beam lithography.[65]

Organic TFTs with patterned metal gate electrodes fabricated using electron-beam lithography on non-conducting substrates were first reported in 2011 by Frederik Ante et al.[66] and Michael Novak et al.[67] In addition to channel lengths of about 100 nm, these TFTs also had submicron gate-to-source and gate-to-drain overlaps and a small gate-dielectric thickness (**Figure 8**). The latter is important to ensure that even for small channel lengths, the electric-potential distribution and the charge–carrier density in the semiconductor are still controlled mainly by the transverse gate field, rather than the lateral drain–source field. According to the scaling laws developed for silicon MOSFETs,[68,69] the ratio between the channel length and the gate-dielectric thickness should always be greater than about 10. For a channel length of 100 nm, this implies a gate-dielectric thickness of less than 10 nm.

The first flexible organic TFTs fabricated using electron-beam lithography were reported by Ute Zschieschang et al. in 2022.[70] TFTs with channel lengths ranging from 200 to 900 nm and gate-to-contact overlaps of 100 or 200 nm were fabricated on flexible PEN. The TFTs were implemented in the inverted coplanar (bottom-gate, bottom-contact) device architecture. Owing in part to the relatively small gate-dielectric thickness (8 nm) and large unit-area gate-dielectric capacitance (0.7 µF cm^{-2}),[71] the TFTs displayed good static characteristics (despite the small lateral dimensions), including on/off current ratios between 5×10^6 and 4×10^9 and subthreshold swings between 70 and 200 mV/decade. In addition to individual TFTs, the authors also fabricated unipolar inverters (based on two p-channel TFTs with a channel length of 200 nm and gate-to-contact overlaps of 100 nm) on a glass substrate. From the inverter's output signal measured in response to a square-wave signal applied to the input node, a characteristic time constant (τ) of the signal-propagation delay of 40 ns was extracted, which corresponds to an equivalent frequency [$f_{eq} = 1/(2{\cdot}\tau)$] of 12.5 MHz (at a supply voltage of 2 V).

Using the same process, Tanumita Haldar et al. fabricated unipolar inverters based on p-channel TFTs with a channel length of 120 nm and gate-to-source and gate-to-drain overlaps of 90 nm

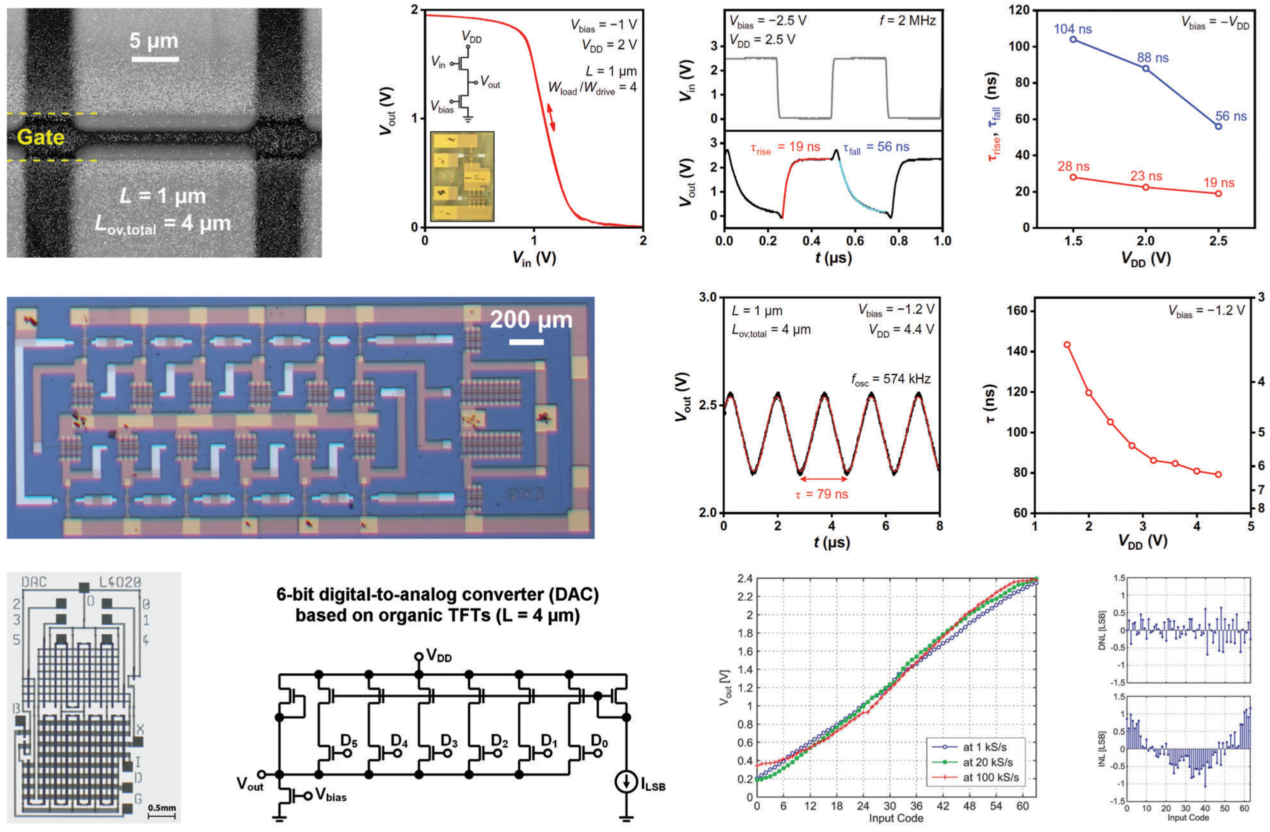

Figure 7. Stencil lithography for high-frequency integrated circuits based on organic TFTs with channel lengths as small as 1 µm, gate-to-contact overlaps as small as 2 µm, signal delays as short as 19 ns, and data conversion rates as high as 100 kS s^{-1} (Tarek Zaki et al.; James Borchert et al.). Top and center: Adapted under the terms of the CC BY-NC license.[52] Copyright 2020, American Association for the Advancement of Science. Bottom: Adapted with permission.[51] Copyright 2012, IEEE.

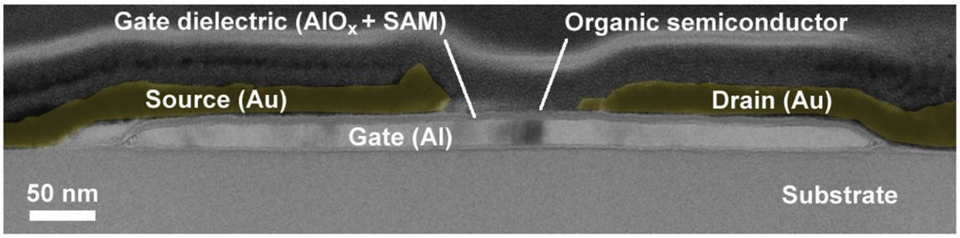

Figure 8. Cross-sectional transmission electron microscopy image of an organic TFT with a channel length of 100 nm and gate-to-contact overlaps of 200 nm fabricated using electron-beam lithography (Frederik Ante et al.). The gate-dielectric thickness is about 7 nm. Adapted with permission.[66] Copyright 2011, Wiley-VCH.

on a flexible PEN substrate.[72] These inverters operated with an equivalent frequency of 36 MHz at a supply voltage of 3 V. This is the highest frequency of operation reported to date for flexible organic TFTs. **Table 4** summarizes the dynamic performance of organic TFTs fabricated using electron-beam lithography, and **Figure 9** illustrates the key results.

In both these reports,[70,72] the dynamic device performance was limited by the relatively large contact resistance of the TFTs fabricated using electron-beam lithography (about 1 kΩcm). A possible explanation for why these TFTs have a larger contact resistance than TFTs fabricated using stencil lithography (even though the device architecture and the functional materials were the same)[52] are the relatively sharp edges of the source/drain contacts when these are patterned by electron-beam lithography, rather than by stencil lithography. The impact of the sharpness of the edges of the source/drain contacts in organic TFTs fabricated in the inverted coplanar (bottom-gate, bottom-contact) device architecture on the contact resistance has been evaluated by Xiaolin Ye et al.[73] According to Equation (1), the large contact resistance negates most of the benefits of the small channel length and gate-to-contact overlaps on the transit frequency of the TFTs fabricated using electron-beam lithography. Assuming the contact resistance can be decreased to approximately the values achieved in organic TFTs fabricated using stencil lithography (10 Ωcm), substantially higher transit frequencies will be possible.

Table 4. Literature summary of organic TFTs fabricated using electron-beam lithography for which operation at frequencies above 10 MHz has been reported.

Author	Ref.	Substrate	Semiconductor	f_T or f_{eq} [MHz]	L [µm]	L_{ov} [µm]	μ_0 [cm^2 V^{-1}s^{-1}]	$R_C W$ [Ωcm]	V_{GS} [V]	V_{th} [V]	C_{diel} [nF cm^{-2}]
Zschieschang	[70]	Glass	DPh-DNTT	12.5	0.2	0.1	1	1000	−2	−0.5	700
Haldar	[72]	Flexible PEN	DPh-DNTT	36	0.12	0.09	1	1100	−3	−0.5	700

The principal advantage of electron-beam lithography is its extremely high resolution. Flexible organic TFTs with channel lengths and gate-to-contact overlaps of 100 nm have already been reported.[70,72] The feasibility of patterning channel lengths as small as a few tens of nanometers has also been demonstrated, albeit thus far only on rigid silicon substrates.[60–63,74] The static current–voltage characteristics of organic TFTs with such small channel lengths will possibly suffer from a less well-defined off-state behavior, including a larger off-state drain current and a larger subthreshold swing, unless the gate-dielectric thickness is decreased to about 5 nm.[67,71] These considerations notwithstanding, the fabrication of flexible organic TFTs with channel lengths and gate-to-contact overlaps as small as about 50 nm and transit frequencies in excess of 100 MHz (and potentially approaching 1 GHz) is entirely feasible with the help of electron-beam lithography. Drawbacks of electron-beam lithography include the high costs of the lithography system, the need for resists and solvents, and the low throughput of single-beam systems.

6. Mix-and-Match Lithography

The gate electrodes and source/drain contacts of most of the TFTs discussed up to this point were patterned using the same lithography method, that is, either photolithography, laser lithography, stencil lithography or electron-beam lithography. The term "mix-and-match lithography" refers to the concept of using different lithography techniques to pattern the various TFT components. In 2014, Takafumi Uemura et al. (University of Tokyo) reported a transit frequency of 20 MHz for organic TFTs fabricated by a combination of photolithography and lift-off for the primary gate electrodes, self-aligned photolithography and lift-off for the secondary ("split") gate electrodes, and shadow-mask lithography (using an extremely thin metal wire as a mask) for the source and drain contacts.[75] The purpose of the split gates is to actively manipulate the contact resistance during device operation by applying additional electric fields near the source and drain regions of the transistors during operation. The TFTs were fabricated in the inverted staggered (bottom-gate, top-contact) device architecture and had a channel length of 2.5 µm, gate-to-contact overlaps of 0.5 µm, a channel-width-normalized contact resistance of 480 Ωcm, and a transit frequency of 20 MHz. **Table 5** provides a summary of the device parameters, and **Figure 10** illustrates the results.

7. Patterning of Organic Semiconductors

The previous sections focused on the patterning of the gate electrodes and the source/drain contacts, since the resolution with which these are patterned is directly relevant to the channel length and the gate-to-contact overlaps and thus to the dynamic performance of the TFTs. Nevertheless, the organic-semiconductor layer must usually be patterned as well, in order to minimize leakage currents and to allow TFTs based on different organic semiconductors (e.g., p-channel and n-channel organic TFTs) to be placed in dense patterns, that is, in close proximity to each other. The requirements in terms of the resolution are generally less critical in this case, so that techniques other than the ones discussed in the previous sections may be considered. However, organic semiconductors tend to be more sensitive to process chemicals than the metals typically employed for the gate electrodes and the source/drain contacts, and this may limit the choice of the patterning approaches. One option are additive processes by which the organic semiconductors are deposited onto the substrate only where needed, for example by inkjet printing,[76] organic vapor-jet printing[77] or vacuum deposition through stencil masks.[50–52,70–72,78] Subtractive patterning of organic semiconductors has been demonstrated as well, for example by using a combination of orthogonal photolithography and oxygen-plasma etching,[79] by exploiting the gate electrodes (of top-gate TFTs) as an etch mask,[80] or by laser ablation.[81]

8. Summary and Outlook

Table 6 summarizes some of the important parameters of organic TFTs for which operation at frequencies above 10 MHz has been experimentally demonstrated as of the writing of this review. The table includes results from both lateral and vertical organic transistors. The highest transit frequency (160 MHz) was reported for lateral organic TFTs fabricated using laser lithography and operating at gate–source and drain–source voltages of 40 V.[43] For low-voltage operation (below 10 V), an equivalent frequency of 100 MHz (signal delay of 5 ns at voltages of 4 V) has been reported for vertical organic permeable-base transistors,[82] and a transit frequency of 45 MHz (at 7 V) has been reported for lateral organic TFTs fabricated using photolithography.[34] The best dynamic performance reported for flexible organic TFTs are transit frequencies of 22 and 21 MHz for TFTs fabricated using laser lithography[42] and stencil lithography,[52] respectively, and an equivalent frequency of 36 MHz (signal delay of 14 ns at voltages of 3 V) reported for TFTs fabricated using electron-beamlithography.[72]

Table 7 provides a brief comparison of the merits and limitations of the four lithography methods discussed in this review.

The strengths of photolithography are the extremely high throughput, the relatively low costs (except for projection lithography), and the possibility of self-alignment of the source and drain contacts with respect to the gate electrode by means of a backside exposure, which is something that none of the other three methods can provide. The principal limitation of

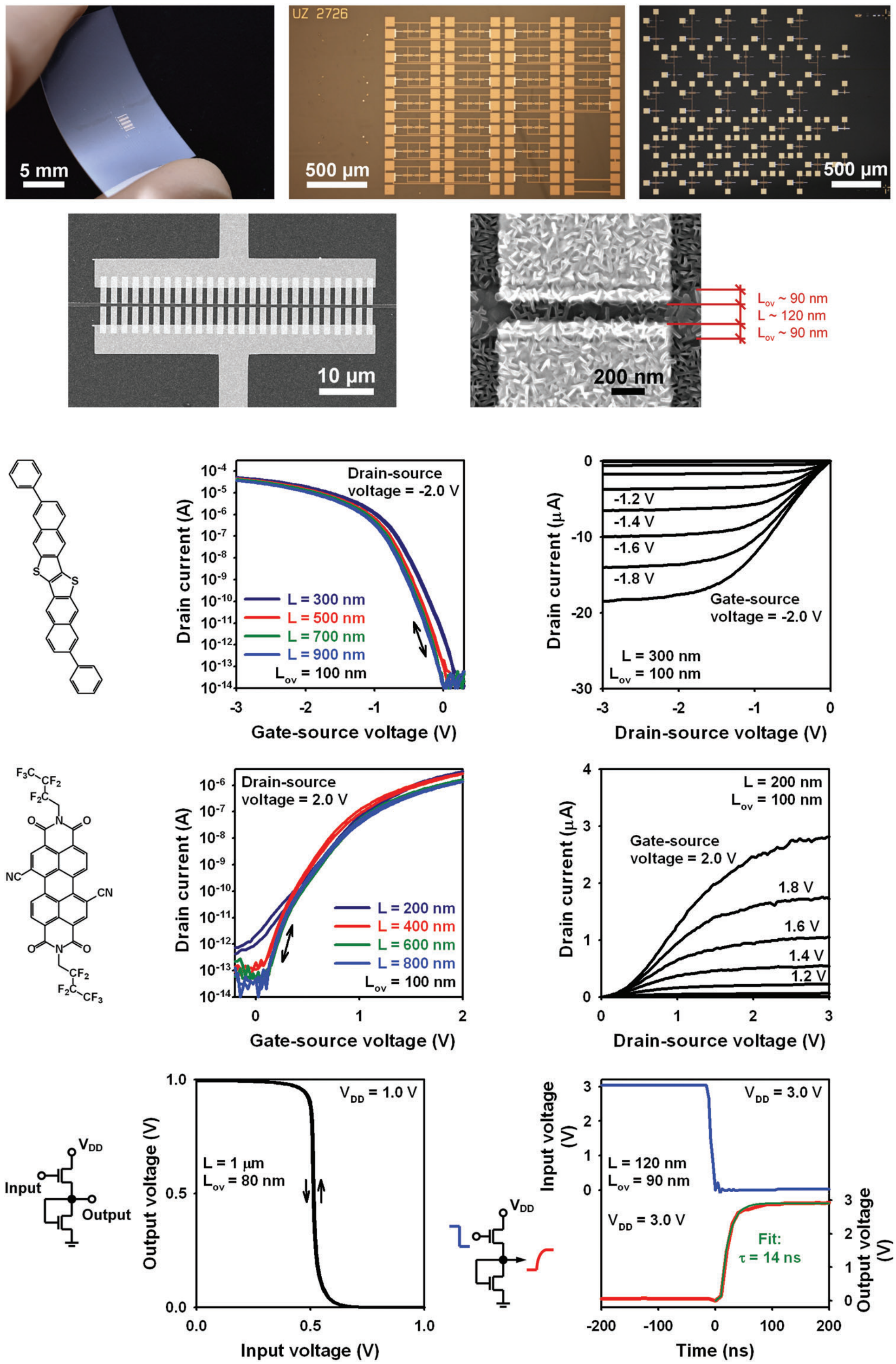

Figure 9. Electron-beam lithography for high-frequency organic TFTs, fabricated on flexible polymeric substrates with channel lengths as small as 120 nm, gate-to-contact overlaps as small as 90 nm, and signal delays as short as 14 ns (Ute Zschieschang et al.; Tanumita Haldar et al.). Adapted under the terms of the CC BY-NC license.[70,72] Top, Copyright 2022, American Association for the Advancement of Science; Bottom, Copyright 2023, American Association for the Advancement of Science.

Table 5. Literature summary of organic TFTs fabricated using mix-and-match lithography for which operation at frequencies above 10 MHz has been reported.

Author	Ref.	Substrate	Semiconductor	f_T or f_{eq} [MHz]	L [µm]	L_{ov} [µm]	μ_0 [$cm^2 V^{-1} s^{-1}$]	$R_C W$ [Ωcm]	V_{GS} [V]	V_{th} [V]	C_{diel} [nF cm^{-2}]
Uemura	[75]	Glass	C_{10}-DNTT	20	2.5	0.5	3.8	480	20	0	24

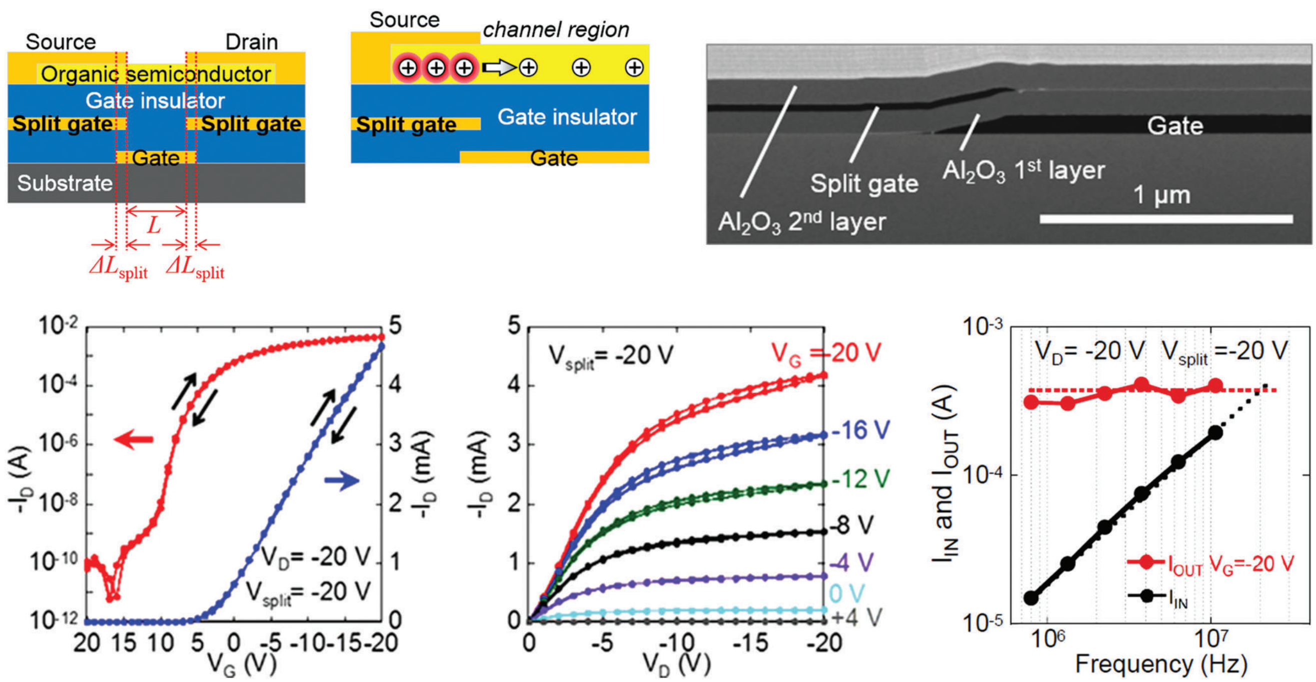

Figure 10. Mix-and-match lithography for high-frequency organic TFTs, fabricated in the inverted staggered (bottom-gate, top-contact) device architecture with a channel length of 2.5 µm, gate-to-contact overlaps of 0.5 µm, and a transit frequency of 20 MHz (Takafumi Uemura et al.). Adapted with permission.[75] Copyright 2014, Wiley-VCH.

photolithography is the resolution, which (except for projection lithography) is no better than about 1 µm. However, with self-alignment, this limitation pertains only to the channel length, not to the gate-to-contact overlaps, which means that despite this limitation, transit frequencies above 1 GHz are entirely feasible using photolithography.

A beneficial feature of laser and stencil lithography is that these two methods do not require resists or solvents, which can be an important advantage if the TFTs and circuits are fabricated on sensitive substrates or using sensitive semiconductors or dielectrics. Laser lithography has the additional benefit of not requiring masks (similar to maskless photolithography), while stencil lithography benefits from high throughput and low system costs (similar to contact or proximity photolithography). The potential of laser and stencil lithography for gigahertz organic TFTs is difficult to assess, since it is not clear how small the channel length and the gate-to-contact overlaps can ultimately be made, but at least for stencil lithography, the lack of a possibility for self-alignment likely puts a transit frequency of 1 GHz out of reach.

Electron-beam lithography provides the ultimate resolution for the channel length while also allowing for extremely small gate-to-contact overlaps, despite the lack of a self-alignment option. Assuming the contact resistance of the TFTs can be decreased to approximately the level routinely achieved in organic TFTs fabricated using other lithography techniques, transit frequencies of 1 GHz are indeed feasible using electron-beam lithography, even for TFTs fabricated on flexible polymeric substrates.

The main drawbacks of laser lithography and electron-beam lithography are the high system costs and the low throughput of single-beam systems. However, regarding the system costs, it might be argued that in commercial manufacturing, the system costs become inconsequential once the production volume is sufficiently high. And the throughput of both laser lithography and electron-beam lithography can be massively increased by expanding the system design from a single beam to arrays of individually addressable beams. For example, more than a dozen different designs for multi-beam, multi-emitter, and multi-column electron-beam-lithography systems have already been developed.[87] The throughput of such systems is just as high as that of commercial photolithography systems, while providing essentially the same high resolution as state-of-the-art single-beam systems. Should such multi-beam systems become more widely available, the commercial manufacturing of integrated circuits using laser or electron-beam lithography may in fact become practical and economical.

Table 6. Complete list of organic TFTs for which operation at frequencies above 10 MHz has been reported. If the gate-to-source and gate-to-drain overlaps are not identical, the average gate-to-contact overlap is given. Note that Equation (1) was derived under the assumption that the gate-to-source and the gate-to-drain overlap lengths are identical ($L_{ov} = L_{ov,GS} = L_{ov,GD}$) and that they have the same influence on the transit frequency, while in reality, $L_{ov,GS}$ and $L_{ov,GD}$ have slightly different impacts on the transit frequency, at least when the TFTs are biased in saturation.[52,54,83]

Author	Ref.	Device architecture	Patterning method for the source/drain contacts	Patterning method for the gate electrodes	f_T or f_{eq} [MHz]	L [µm]	L_{ov} [µm]	V_{GS} [V]	f_T/V_{GS} or f_{eq}/V_{GS} [MHz]
Perinot	[43]	Lateral	Laser lithography	Laser lithography	160	1.2	0.17	40	4
Guo	[82]	Vertical	Shadow-mask lithography	Shadow-mask lithography	100	0.5	n/a	4	25
Sawada	[34]	Lateral	Photolithography	Photolithography	45	1.5	1	−7	6.43
Höppner	[84]	Vertical	Photolithography	Photolithography	43.2	0.2	3	−10	4.32
Kheradmand-B.	[85]	Vertical	Shadow-mask lithography	Shadow-mask lithography	40	0.2	n/a	8.6	4.65
Yamamura	[35]	Lateral	Photolithography	Photolithography	38	1.5	2	−15	2.53
Haldar	[72]	Lateral	Electron-beam lithography	Electron-beam lithography	36	0.12	0.09	−3	12
Kitamura	[24]	Lateral	Photolithography	Photolithography	27.7	2	2.5	20	1.39
Passarella	[42]	Lateral	Laser lithography	Inkjet printing	24	1.4	2.7	−15	1.6
Passarella	[42]	Lateral	Laser lithography	Inkjet printing	22	1.2	2.3	−12	1.83
Borchert	[52]	Lateral	Stencil lithography	Stencil lithography	21	0.6	5	−3	7
Kitamura	[23]	Lateral	Photolithography	Photolithography	20	2	1	20	1
Uemura	[75]	Lateral	Thin-wire shadow masking	Photolithography	20	2.5	0.5	−20	1
Uno	[86]	Vertical	Oblique-angle deposition	Photolithography	20	0.8	n/a	−15	1.33
Perinot	[39]	Lateral	Laser lithography	Inkjet printing	20	1.75	3	30	0.67
Yamamura	[33]	Lateral	Photolithography	Photolithography	20	3	2.25	−10	2
Nakayama	[32]	Lateral	Photolithography	Photolithography	19	2	2	−10	1.9
Giorgio	[41]	Lateral	Laser lithography	Inkjet printing	19	1.2	2.3	12	1.58
Perinot	[40]	Lateral	Laser lithography	Inkjet printing	14.4	1	1.7	7	2.06
Zschieschang	[70]	Lateral	Electron-beam lithography	Electron-beam lithography	12.5	0.2	0.1	−2	6.25
Kitamura	[24]	Lateral	Photolithography	Photolithography	11.4	2	2.5	−20	0.57
Zschieschang	[53]	Lateral	Stencil lithography	Stencil lithography	10.4	0.85	5	−3	3.47

Table 7. Merits and limitations of the four lithography techniques that have been employed for the fabrication of the high-frequency organic TFTs.

	Photo-lithography	Laser lithography	Stencil lithography	Electron-beam lithography
Smallest channel length reported for flexible organic TFTs	2 µm	1 µm	0.6 µm	120 nm
Resolution limit (rough estimate)	1 µm (contact/maskless) <100 nm (projection)	1 µm	<1 µm	<100 nm
Throughput	Extremely high	Low	High	Low
Masks required?	Yes (contact/proximity) No (maskless)	No	Yes	No
Resists/solvents required?	Yes	No	No	Yes
Equipment costs	Low (contact/maskless) Exorbitant (projection)	High	Low	High
Mask costs	Low (contact/proximity) Zero (maskless)	Zero	High	Zero
Self-alignment possible?	Yes	No	No	No
Potential for $f_T \geq 1$ GHz ($R_C W = 10\ \Omega$cm, $V_{GS} - V_{th} = 5$ V)	Yes ($L = 1$ µm, $L_{ov} = 0$, i.e., with self-alignment)	Possibly ($L = 800$ nm, $L_{ov} = 100$ nm)	Unlikely (would require $L_{ov} < 1$ µm, which is probably not feasible)	Yes (L, $L_{ov} \leq 500$ nm)

As a final note, it is worth pointing out again that in the commercial manufacturing of silicon MOSFETs, which represent the most successful type of semiconductor device to date, the by far most critical process steps are those in which the transistor components are lithographically patterned. It is important to understand that for organic TFTs to eventually find use in high-volume commercial applications, a similar emphasis on high-resolution lithography may be critical. This is what we hope to accomplish with this review.

Acknowledgements

The authors would like to thank Kazuo Takimiya (RIKEN Center for Emergent Matter Science, Wako, Saitama, Japan) as well as Koichi Ikeda, Yuichi Sadamitsu, and Satoru Inoue (Nippon Kayaku, Tokyo, Japan) for providing the organic semiconductor DPh-DNTT for the work described in Sections 4 and 5. This work was partially funded by the German Research Foundation (DFG) under the grants KL 2223/6-1 and KL 2223/6-2 (SPP FFlexCom), and KL 2223/7-1 and INST 35/1429-1 (SFB 1249).

Open access funding enabled and organized by Projekt DEAL.

Conflict of Interest

The authors declare no conflict of interest.

Keywords

high-resolution lithography, organic transistors, transit frequency

Received: November 7, 2022
Revised: February 7, 2023
Published online: April 4, 2023

[1] R. A. Street, *Adv. Mater.* **2009**, *21*, 2007.
[2] L. Han, P. Mandlik, K. H. Cherenack, S. Wagner, *Appl. Phys. Lett.* **2009**, *94*, 162105.
[3] T.-C. Chang, Y.-C. Tsao, P.-H. Chen, M.-C. Tai, S.-P. Huang, W.-C. Su, G.-F. Chen, *Mater. Today Adv.* **2020**, *5*, 100040.
[4] J. Troughton, D. Atkinson, *J. Mater. Chem. C* **2019**, *7*, 12388.
[5] J. Lee, T. T. Nguyen, J. Bae, G. Jo, Y. Lee, S. Yang, H. Chu, J. Kwag, *J. Soc. Inf. Disp.* **2018**, *26*, 200.
[6] A. R. Cowen, S. M. Kengyelics, A. G. Davies, *Clin. Radiol.* **2008**, *63*, 487.
[7] N. Münzenrieder, G. Cantarella, L. Petti, *ECS Trans.* **2019**, *1*, 55.
[8] B. Hekmatshoar, K. H. Cherenack, A. Z. Kattamis, K. Long, S. Wagner, J. C. Sturm, *Appl. Phys. Lett.* **2008**, *93*, 032103.
[9] X. Gao, L. Lin, Y. Liu, X. Huang, *J. Disp. Technol.* **2015**, *11*, 666.
[10] C. Wang, H. Dong, W. Hu, Y. Liu, D. Zhu, *Chem. Rev.* **2012**, *112*, 2208.
[11] S. Steudel, K. Myny, S. Schols, P. Vicca, S. Smout, A. Tripathi, B. van der Putten, J.-L. van der Steen, M. van Neer, F. Schütze, O. R. Hild, E. van Veenendaal, P. van Lieshout, M. van Mil, J. Genoe, G. Gelinck, P. Heremans, *Org. Electron.* **2012**, *13*, 1729.
[12] H. M. Kim, H. W. Kang, D. K. Hwang, H. S. Lim, B.-K. Ju, J. A. Lim, *Adv. Funct. Mater.* **2016**, *26*, 2706.
[13] U. Zschieschang, H. Klauk, *J. Mater. Chem. C* **2019**, *7*, 5522.
[14] Y. Kubota, T. Matsumoto, H. Tsuji, N. Suzuki, S. Imai, H. Kobayashi, *IEEE Trans. Electron Devices* **2012**, *59*, 385.
[15] T. Zaki, R. Rödel, F. Letzkus, H. Richter, U. Zschieschang, H. Klauk, J. N. Burghartz, *IEEE Electron Device Lett.* **2013**, *34*, 520.
[16] A. F. Paterson, S. Singh, K. J. Fallon, T. Hodsden, Y. Han, B. C. Schroeder, H. Bronstein, M. Heeney, I. McCulloch, T. D. Anthopoulos, *Adv. Mater.* **2018**, *30*, 1801079.
[17] J. W. Borchert, R. T. Weitz, S. Ludwigs, H. Klauk, *Adv. Mater.* **2022**, *34*, 2104075.
[18] B. Lüssem, A. Günther, A. Fischer, D. Kasemann, K. Leo, *J. Phys.: Condens. Matter* **2015**, *27*, 443003.
[19] H. Kleemann, K. Krechan, A. Fischer, K. Leo, *Adv. Funct. Mater.* **2020**, *30*, 1907113.
[20] Y. Chen, Y. Yao, N. Turetta, P. Samori, *J. Mater. Chem. C* **2022**, *10*, 2494.
[21] R. P. Seisyan, *Tech. Phys.* **2011**, *56*, 1061.
[22] D. J. Gundlach, T. N. Jackson, D. G. Schlom, S. F. Nelson, *Appl. Phys. Lett.* **1999**, *74*, 3302.
[23] M. Kitamura, Y. Arakawa, *Appl. Phys. Lett.* **2009**, *95*, 023503.
[24] M. Kitamura, Y. Arakawa, *Jpn. J. Appl. Phys.* **2011**, *50*, 01BC01.
[25] K. Myny, S. Steudel, S. Smout, P. Vicca, F. Furthner, B. van der Putten, A. K. Tripathi, G. H. Gelinck, J. Genoe, W. Dehaene, P. Heremans, *Org. Electron.* **2010**, *11*, 1176.
[26] K. Myny, M. J. Beenhakkers, N. A. J. M. van Aerle, G. H. Gelinck, J. Genoe, W. Dehaene, P. Heremans, *IEEE J. Solid-State Circuits* **2011**, *46*, 1223.
[27] K. Myny, E. van Veenendaal, G. H. Gelinck, J. Genoe, W. Dehaene, P. Heremans, *IEEE J. Solid-State Circuits* **2012**, *47*, 284.
[28] D. Raiteri, P. van Lieshout, A. van Roermund, E. Cantatore, *IEEE J. Solid-State Circuits* **2014**, *49*, 524.
[29] M. Noda, N. Kobayashi, M. Katsuhara, A. Yumoto, S. Ushikura, R. Yasuda, N. Hirai, G. Yukawa, I. Yagi, K. Nomoto, T. Urabe, *J. Soc. Inf. Disp.* **2011**, *19*, 316.
[30] S. Kumagai, T. Makita, S. Watanabe, J. Takeya, *Appl. Phys. Express* **2022**, *15*, 030101.
[31] P. G. Taylor, J. K. Lee, A. A. Zakhidov, M. Chatzichristidi, H. H. Fong, J. A. DeFranco, G. G. Malliaras, C. K. Ober, *Adv. Mater.* **2009**, *21*, 2314.
[32] K. Nakayama, M. Uno, T. Uemura, N. Namba, Y. Kanaoka, T. Kato, M. Katayama, C. Mitsui, T. Okamoto, J. Takeya, *Adv. Mater. Interfaces* **2014**, *1*, 1300124.
[33] A. Yamamura, S. Watanabe, M. Uno, M. Mitani, C. Mitsui, J. Tsurumi, N. Isahaya, Y. Kanaoka, T. Okamoto, J. Takeya, *Sci. Adv.* **2018**, *4*, eaao5758.
[34] T. Sawada, A. Yamamura, M. Sasaki, K. Takahira, T. Okamoto, S. Watanabe, J. Takeya, *Nat. Commun.* **2020**, *11*, 4839.
[35] A. Yamamura, T. Sakon, K. Takahira, T. Wakimoto, M. Sasaki, T. Okamoto, S. Watanabe, J. Takeya, *Adv. Funct. Mater.* **2020**, *30*, 1909501.
[36] H. Gold, A. Haase, A. Fian, C. Prietl, B. Striedinger, F. Zanella, N. Marjanovic, R. Ferrini, J. Ring, K. D. Lee, R. Jiawook, A. Drost, M. König, R. Müller, K. Myny, J. Genoe, U. Kleb, H. Hirshy, R. Pretot, J. Kraxner, R. Schmied, B. Stadlober, *Org. Electron.* **2015**, *22*, 140.
[37] U. Palfinger, C. Auner, H. Gold, A. Haase, J. Kraxner, T. Haber, M. Sezen, W. Grogger, G. Domann, G. Jakopic, J. R. Krenn, B. Stadlober, *Adv. Mater.* **2010**, *22*, 5115.
[38] S. G. Higgins, B. V. O. Muir, G. Dell'Erba, A. Perinot, M. Caironi, A. J. Campbell, *Appl. Phys. Lett.* **2016**, *108*, 023302.
[39] A. Perinot, P. Kshirsagar, M. A. Malvindi, P. P. Pompa, R. Fiammengo, M. Caironi, *Sci. Rep.* **2016**, *6*, 38941.
[40] A. Perinot, M. Caironi, *Adv. Sci.* **2019**, *6*, 1801566.
[41] M. Giorgio, M. Caironi, *IEEE Electron Device Lett.* **2019**, *40*, 953.
[42] B. Passarella, A. D Scaccabarozzi, M. Giorgio, A. Perinot, S. M. Barbier, J. Martin, M. Caironi, *Flexible Printed Electron.* **2020**, *5*, 034001.
[43] A. Perinot, M. Giorgio, V. Mattoli, D. Natali, M. Caironi, *Adv. Sci.* **2021**, *8*, 2001098.
[44] O. Vazquez-Mena, L. Gross, S. Xie, L. G. Villanueva, J. Brugger, *Microelectron. Eng.* **2015**, *132*, 236.

[45] S.-K. Hong, J.-H. Sim, I.-G. Seo, K.-C. Kim, S.-I. Bae, H.-Y. Lee, N.-Y. Lee, J. Jang, *J. Disp. Technol.* **2010**, *6*, 601.
[46] T. A. Mai, B. Richerzhagen, *2007 Int. Symp. Soc. Inf. Disp. (SID)* **2007**, *38*, 1596.
[47] G. M. Kim, M. A. F. van den Boogaart, J. Brugger, *Microelectron. Eng.* **2003**, *67–68*, 609.
[48] F. Letzkus, J. Butschke, B. Höfflinger, M. Irmscher, C. Reuter, R. Springer, A. Ehrmann, J. Mathuni, *Microelectron. Eng.* **2000**, *53*, 609.
[49] J. Melngailis, A. A. Mondelli, I. L. Berry III, R. Mohondroa, *J. Vac. Sci. Technol. B* **1998**, *16*, 927.
[50] K. Sidler, N. V. Cvetkovic, V. Savu, D. Tsamados, A. M. Ionescu, J. Brugger, *Sens. Actuators A* **2010**, *162*, 336.
[51] T. Zaki, F. Ante, U. Zschieschang, J. Butschke, F. Letzkus, H. Richter, H. Klauk, J. N. Burghartz, *IEEE J. Solid-State Circuits* **2012**, *47*, 292.
[52] J. W. Borchert, U. Zschieschang, F. Letzkus, M. Giorgio, R. T. Weitz, M. Caironi, J. N. Burghartz, S. Ludwigs, H. Klauk, *Sci. Adv.* **2020**, *6*, eaaz5156.
[53] U. Zschieschang, J. W. Borchert, M. Giorgio, M. Caironi, F. Letzkus, J. N. Burghartz, U. Waizmann, J. Weis, S. Ludwigs, H. Klauk, *Adv. Funct. Mater.* **2020**, *30*, 1903812.
[54] J. Leise, J. Pruefer, G. Darbandy, A. Nikolaou, M. Giorgio, M. Caironi, U. Zschieschang, H. Klauk, A. Kloes, B. Iñiguez, J. W. Borchert, *J. Appl. Phys.* **2021**, *130*, 125501.
[55] O. Vazquez-Mena, L. G. Villanueva, V. Savu, K. Sidler, P. Langlet, J. Brugger, *Nanotechnology* **2009**, *20*, 415303.
[56] U. Zschieschang, J. W. Borchert, M. Geiger, F. Letzkus, J. N. Burghartz, H. Klauk, *Org. Electron.* **2018**, *61*, 65.
[57] U. Zschieschang, F. Letzkus, J. N. Burghartz, H. Klauk, *IEEE Trans. Nanotechnol.* **2017**, *16*, 837.
[58] V. R. Manfrinato, A. Stein, L. Zhang, C.-Y. Nam, K. G. Yager, E. A. Stach, C. T. Black, *Nano Lett.* **2017**, *17*, 4562.
[59] E. L. Granstrom, C. D. Frisbie, *J. Phys. Chem. B* **1999**, *103*, 8842.
[60] J. Collet, O. Tharaud, A. Chapoton, D. Vuillaume, *Appl. Phys. Lett.* **2000**, *76*, 1941.
[61] Y. Zhang, J. R. Petta, S. Ambily, Y. Shen, D. C. Ralph, G. G. Malliaras, *Adv. Mater.* **2003**, *15*, 1632.
[62] L. Wang, D. Fine, T. Jung, D. Basu, H. von Seggern, A. Dodabalapur, *Appl. Phys. Lett.* **2004**, *85*, 1772.
[63] J. Lee, P. C. Chang, J. A. Liddle, V. Subramanian, *IEEE Trans. Electron Devices* **2005**, *52*, 1874.
[64] M. Mottaghi, P. Lang, F. Rodriguez, A. Rumyantseva, A. Yassar, G. Horowitz, S. Lenfant, D. Tondelier, D. Vuillaume, *Adv. Funct. Mater.* **2007**, *17*, 597.
[65] V. Wagner, P. Wöbkenberg, A. Hoppe, J. Seekamp, *Appl. Phys. Lett.* **2006**, *89*, 243515.
[66] F. Ante, D. Kälblein, U. Zschieschang, T. W. Canzler, A. Werner, K. Takimiya, M. Ikeda, T. Sekitani, T. Someya, H. Klauk, *Small* **2011**, *7*, 1186.
[67] M. Novak, A. Ebel, T. Meyer-Friedrichsen, A. Jedaa, B. F. Vieweg, G. Yang, K. Voitchovsky, F. Stellacci, E. Spiecker, A. Hirsch, M. Halik, *Nano Lett.* **2011**, *11*, 156.
[68] R. H. Dennard, F. H. Gaensslen, H.-N. Yu, V. L. Rideout, E. Bassous, A. R. LeBlanc, *IEEE J. Solid-State Circuits* **1974**, *9*, 256.
[69] G. Baccarani, M. R. Wordeman, R. H. Dennard, *IEEE Trans. Electron Devices* **1984**, *31*, 452.
[70] U. Zschieschang, U. Waizmann, J. Weis, J. W. Borchert, H. Klauk, *Sci. Adv.* **2022**, *8*, eabm9845.
[71] M. Geiger, M. Hagel, T. Reindl, J. Weis, R. T. Weitz, H. Solodenko, G. Schmitz, U. Zschieschang, H. Klauk, R. Acharya, *Sci. Rep.* **2021**, *11*, 6382.
[72] T. Haldar, T. Wollandt, J. Weis, U. Zschieschang, H. Klauk, R. T. Weitz, J. N. Burghartz, M. Geiger, *Sci. Adv.* **2023**, *9*, eadd3669.
[73] X. Ye, X. Zhao, S. Wang, Z. Wei, G. Lv, Y. Yang, Y. Tong, Q. Tang, Y. Liu, *ACS Nano* **2021**, *15*, 1155.
[74] M. Brouillard, N. Bercu, U. Zschieschang, O. Simonetti, R. Mittapalli, H. Klauk, L. Giraudet, *Nanoscale Adv.* **2022**, *4*, 2018.
[75] T. Uemura, T. Matsumoto, K. Miyake, M. Uno, S. Ohnishi, T. Kato, M. Katayama, S. Shinamura, M. Hamada, M.-J. Kang, K. Takimiya, C. Mitsui, T. Okamoto, J. Takeya, *Adv. Mater.* **2014**, *26*, 2983.
[76] J. Kwon, Y. Takeda, R. Shiwaku, S. Tokito, K. Cho, S. Jung, *Nat. Commun.* **2019**, *10*, 54.
[77] S. Kim, H. Moon, H. Kwon, G. Lee, D. Yu, J. Choi, J. Park, S. J. Kim, S. Yoo, *Adv. Mater.* **2019**, *4*, 1800332.
[78] U. Kraft, T. Zaki, F. Letzkus, J. N. Burghartz, E. Weber, B. Murmann, H. Klauk, *Adv. Electron. Mater.* **2019**, *5*, 1800453.
[79] S. Abdinia, T.-H. Ke, M. Ameys, J. Li, S. Steudel, J. L. Vandersteen, B. Cobb, F. Torricelli, A. van Roermund, E. Cantatore, *J. Disp. Technol.* **2015**, *11*, 564.
[80] M. Li, Z. Liu, L. Feng, J. Fan, L. Han, S. Ogier, H. Zhou, X. Guo, *IEEE Electron Device Lett.* **2020**, *41*, 70.
[81] T. Sawada, T. Makita, A. Yamamura, M. Sasaki, Y. Yoshimura, T. Hayakawa, T. Okamoto, S. Watanabe, S. Kumagai, J. Takeya, *Appl. Phys. Lett.* **2020**, *117*, 033301.
[82] E. Guo, S. Xing, F. Dollinger, R. Hübner, S.-J. Wang, Z. Wu, K. Leo, H. Kleemann, *Nat. Electron.* **2021**, *4*, 588.
[83] T. Zaki, R. Rödel, F. Letzkus, H. Richter, U. Zschieschang, H. Klauk, J. N. Burghartz, *Org. Electron.* **2013**, *14*, 1318.
[84] M. Höppner, B. Kheradmand-Boroujeni, J. Vahland, M. F. Sawatzki, D. Kneppe, F. Ellinger, H. Kleemann, *Adv. Sci.* **2022**, *9*, 2201660.
[85] B. Kheradmand-Boroujeni, M. P. Klinger, A. Fischer, H. Kleemann, K. Leo, F. Ellinger, *Sci. Rep.* **2018**, *8*, 7643.
[86] M. Uno, B. S. Cha, Y. Kanaoka, J. Takeya, *Org. Electron.* **2015**, *20*, 119.
[87] M. Esashi, H. Miyaguchi, A. Kojima, N. Ikegami, N. Koshida, H. Ohyi, *Jpn. J. Appl. Phys.* **2022**, *61*, SD0807.

Ute Zschieschang received a Diplom-Ingenieur degree in Mechanical Engineering from Mittweida University of Applied Sciences (FH), Germany, in 2000 and a Ph.D. degree in Chemistry from the Technical University Bergakademie Freiberg, Germany, in 2006. Since 2005, she has been a senior scientist in the Organic Electronics group at the Max Planck Institute for Solid State Research in Stuttgart, Germany.

Hagen Klauk received a Diplom-Ingenieur degree in Electrical Engineering from Chemnitz University of Technology, Germany, in 1995 and a Ph.D. degree in Electrical Engineering from the Pennsylvania State University in 1999. From 1999 to 2000, he was a postdoc at the Center for Thin Film Devices at the Pennsylvania State University. From 2000 to 2005, he was at Infineon Technologies, Erlangen, Germany. Since 2005, he has been head of the Organic Electronics group at the Max Planck Institute for Solid State Research, Stuttgart, Germany.

James W. Borchert received a B.A. degree in Physics from Rutgers University, U.S.A., in 2012 and a M.Sc.Eng. degree in Materials Science and Engineering from the University of Pennsylvania, U.S.A., in 2013. From 2013 to 2015, he worked as a Staff Scientist at Innova Dynamics in San Francisco, California, U.S.A., before completing a Ph.D. degree in Materials Science at the Max Planck Institute for Solid State Research and the University of Stuttgart, Germany, in 2020. In 2020, he joined the 1st Institute of Physics at the Georg August University of Göttingen, Germany, as a postdoc.